Development of Phase-Separated Scintillators with Light-Guiding Properties and their Application for High-Resolution X-ray Imaging

	おお はし　よし ひろ
氏　　名	大　橋　　良　太
研究科，専攻の名称	東北大学大学院工学研究科（博士課程）材料システム工学専攻
学 位 論 文 題 目	Development of Phase-Separated Scintillators with Light-Guiding Properties and their Application for High-Resolution X-ray Imaging. (光導波機能を有する相分離シンチレータ材料の開発と高分解能X線イメージングへの応用に関する研究)
論 文 審 査 委 員	主査　東北大学教授　吉川　彰　　東北大学教授　後藤　孝 東北大学教授　山根 久典　　東北大学教授　増本　博

論文内容要約

Chapter 1. Introduction

In high-resolution radiation imaging systems based on inorganic scintillators, a scintillation light must be guided to the photo-sensors efficiently without lateral light diffusion to achieve the high resolution imaging. Future X-ray imaging applications require a higher spatial resolution with micrometer scale over a wide X-ray energy range. Particularly indirect flat panel detector, which is composed of a scintillator layer and photo-sensor array, requires improvements in their sensitivity and spatial resolution. High sensitivity can be achieved by using a sufficiently thick scintillator layer to absorb the incident X-ray energy completely. However, conventional scintillators, such as Gd_2O_2S:Tb (GOS) powder screens, and even CsI:Tl columnar films reduce the spatial resolution because increasing the thickness causes more light scattering due to the insufficient separation between columns as well as their sidewall roughness. To achieve high sensitivity compatible with high-resolution imaging over a wide radiation energy range, the scintillator layer must possess perfect light guiding properties.

In this study, a new concept of a phase-separated scintillator (PSS) with ideal light guiding property is proposed. The PSS is composed of regular directionally solidified eutectic (DSE) materials with unidirectionally aligned smooth cylinders embedded in a matrix phase. The cylinders usually grow vertically on a solid-liquid interface, and these uniform structures are expected to guide light effectively. The main purpose of this thesis is to develop various PSSs with effective light-guiding properties and to demonstrate a high-resolution X-ray imaging by using them.

Chapter 2. Concept of the Phase-Separated Scintillator (PSS)

This chapter described the capability of a concept of the PSS by simulations. The light-receiving efficiency for various refractive indices of the cylinders and matrix were calculated from the light flux collection efficiencies of the emitted light. From the calculations, two types of possible PSSs were suggested owing to the refractive index ratio (n_m/n_c) of the cylinders (n_c) and the matrix (n_m): matrix-guided PSSs ($n_m/n_c > 1$) and cylinder-guided PSSs ($n_m/n_c < 1$). In the both types, the scintillation lights were transported along the cylinder direction by optical reflection with a total reflection mode between the smooth boundaries with deferent refractive indices, and the light-guiding efficiency increased as increasing the refractive index ratio (n_m/n_c). In the matrix-guided PSSs, scintillation light was guided in the matrix phase with higher refractive index, so that the emitted light was partly diffused in the matrix phase due to its continuous structure, and the high volume fraction of the cylindrical phase was important for improving the light guiding efficiency because it produced sufficient multiple reflections. Whereas, the cylinder-guided PSS had light-guiding properties confined to the cylinders, so that it had better light-guiding property than matrix-guided PSSs because of its strictly confined light-guiding behavior like an optical fiber.

Chapter 3. Matrix-guided PSSs

This chapter described the fabrication of various matrix-guided PSSs and the X-ray imaging results by using them. Various matrix-guided PSSs were fabricated from alkali halide based DSEs. Among them, the CsI-NaCl PSS (CsI:NaCl = 69:31 mol%) consists of the CsI scintillator matrix ($n \approx 1.79$) and NaCl cylinders ($n \approx 1.54$) was a potential matrix-guided PSS because the CsI matrix phase works as an effective scintillator and its fabrication feasibility. A schematic of the CsI-NaCl PSS is shown in Fig.1(a) and prepared CsI-NaCl eutectic is shown in Fig.1(b). Characters beneath the sample were guided to the sample surface because lights were guided along the straight cylinders oriented normal to the surface. An optical transmission images is shown in Fig.1(c). The CsI matrix appeared brighter than the NaCl cylinders because CsI matrix with high refractive index guide light from the back of the crystal to the front. By using Czochralski method, Tl-doped CsI-NaCl PSS crystal that was uniform with no grain boundaries greater than 30 mm in diameter was successfully grown by creating a convex solid/liquid interface, selecting a single grain, and increasing the diameter of the composite moderately.

In addition, the porous cuprous iodide (CuI) scintillator containing aligned cylindrical micropores with a volume fraction of 30% was fabricated by leaching the CuI/KCl PSS (CuI:KCl = 73:27 mol%) in water. The KCl cylinders readily dissolve in water, whereas the CuI matrix is insoluble, therefore cylinder phases were selectively removed by immersing in water. The porous CuI is one of the matrix-guided PSSs and it behaved as efficient light waveguide scintillators due to its high refractive index ratio ($n_m/n_c \approx 2.35$).

A X-ray imaging of a resolution chart of 0.05-mm-thick lead with a 10 line-pairs/mm (lp/mm) pattern was demonstrated by using a CsI–NaCl:Tl PSS and porous CuI scintillator. Contrast transfer function (CTF) values of 10 line-pairs (lp)/mm were 6% for a 420-μm-thick CsI–NaCl:Tl PSS, while the 30% pore volume porous CuI showed better CTF value of 11% for a 800-μm-thick sample. This CTF value of the porous CuI might be the limit of the matrix-guided PSSs because it has relatively higher refractive index ratio and higher volume fraction of cylinder phases than other matrix-guided PSSs.

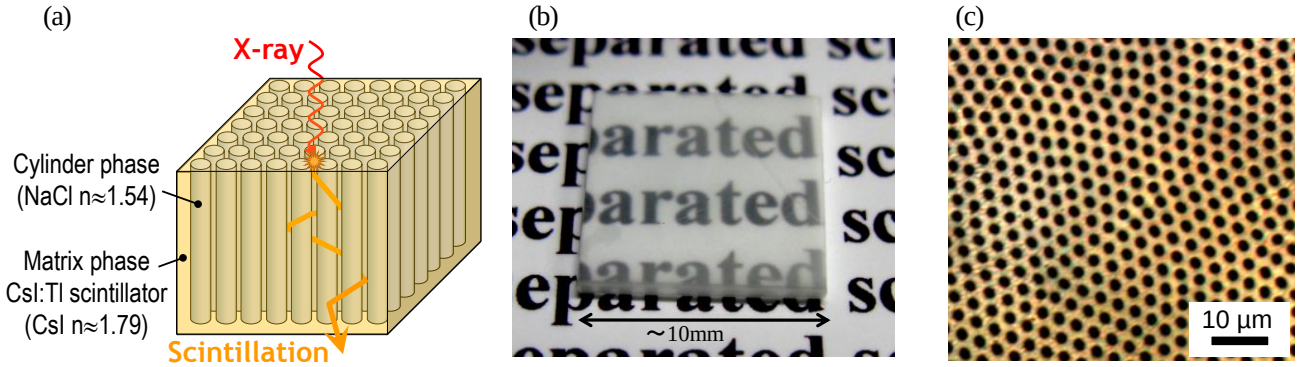

Fig.1. Matrix-guided CsI-NaCl PSS: (a) Schematic illustration, (b) appearance of the CsI-NaCl eutectic crystal, and (c) optical transmission microscope image.

Chapter 4. Cylinder-guided GAP-Al_2O_3 PSS

This chapter described the fabrication of a cylinder-guided $GdAlO_3$ (GAP [gadolinium aluminum perovskite])-Al_2O_3 PSS and its structural, luminescence and optical properties were investigated. A cylinder-guided Ce^{3+}-doped GAP-Al_2O_3 PSS (GAP:Al_2O_3 = 46:54 mol%) consists of the hexagonally well-aligned 680-nm-diameter GAP:Ce^{3+} scintillator cylinders surrounded with α-Al_2O_3 was succesfully fabricated by maintaing the orientation relationship between the *c*-axis of Al_2O_3 matrix and the growth direction of unidirectional solidification. A schematic of the GAP-Al_2O_3 PSS is shown in Fig.2(a) and its appearance and microstructure are shown in Fig.2(b). The GAP scintillator cylinders have a higher refractive index ($n \approx 2.05$) than surrounding Al_2O_3 matrix ($n \approx 1.79$), so that they served as an optical fiber with multi-mode guiding of visible light as shown in Fig.2(c). The image of the lines beneath the sample appears to float on the top surface of the sample, like a fiber optic plate. When irradiated with X-rays, the GAP scintillator cylinders convert X-rays to

light, and emitted light is confined and transported along the cylinder direction in the total reflection mode between GAP/Al_2O_3 boundaries without light-scattering.

The structural analyses revealed that the majority of GAP cylinders had the orientation relationships of [010]GAP//[0001]Al_2O_3 to the growth direction and (100)GAP//(11$\bar{2}$0)Al_2O_3 to the interface plane, while slight misorientation angle of both [010]GAP axis and (100)GAP plane were observed. The EBSD orientation maps is shown in Fig.2(d). The misorientaion of each GAP cylinder could be explained by the other sets of preferable lattice matching between the two phases. The tilt of [010]GAP axis toward the [001]GAP direction could be derived from the competition between (020)GAP//(0006)Al_2O_3 and (022)GAP//(0006)Al_2O_3. The rotation of (100)GAP plane could be derived from the competition between (100)GAP//(11$\bar{2}$0)Al_2O_3 and (101)GAP//(01$\bar{1}$0)Al_2O_3. A few observed minor orientations could be also explained by the other preferable lattice matching. In the GAP/Al_2O_3 interface, a relatively large lattice misfit between the two phases was relieved by insertion of extra half-planes on the Al_2O_3 side of the interface. These structural analyses indicate that the essential growth parameter for the fabrication of a GAP/Al_2O_3 eutectic composite with well-aligned fibrous microstructure is the correspondence between the *c*-axis of Al_2O_3 matrix and the growth direction of unidirectional solidification.

The cathodoluminescence (CL) spectra of individual GAP cylinders showed typical 5d-4f emission band of GAP:Ce^{3+}, while their spectral shape and emission peak showed evident variations. It is considered that these emission variations could be originated from the different orientation relationship of GAP cylinders with Al_2O_3 matrix, which induces slight lattice distortion and changes in the local crystal-field strength of Ce^{3+}, and consequently emission band variations were emerged. Whereas, the CL spectra of Al_2O_3 phase showed intrinsic F^+-center emission, however, its emission was not observed in radioluminescence spectrum of a bulk eutectic composite due to mainly the low attenuation coefficient of Al_2O_3 phase, additionally the spectral overlapping between emission band of F^+-center and excitation/emission bands of GAP phase.

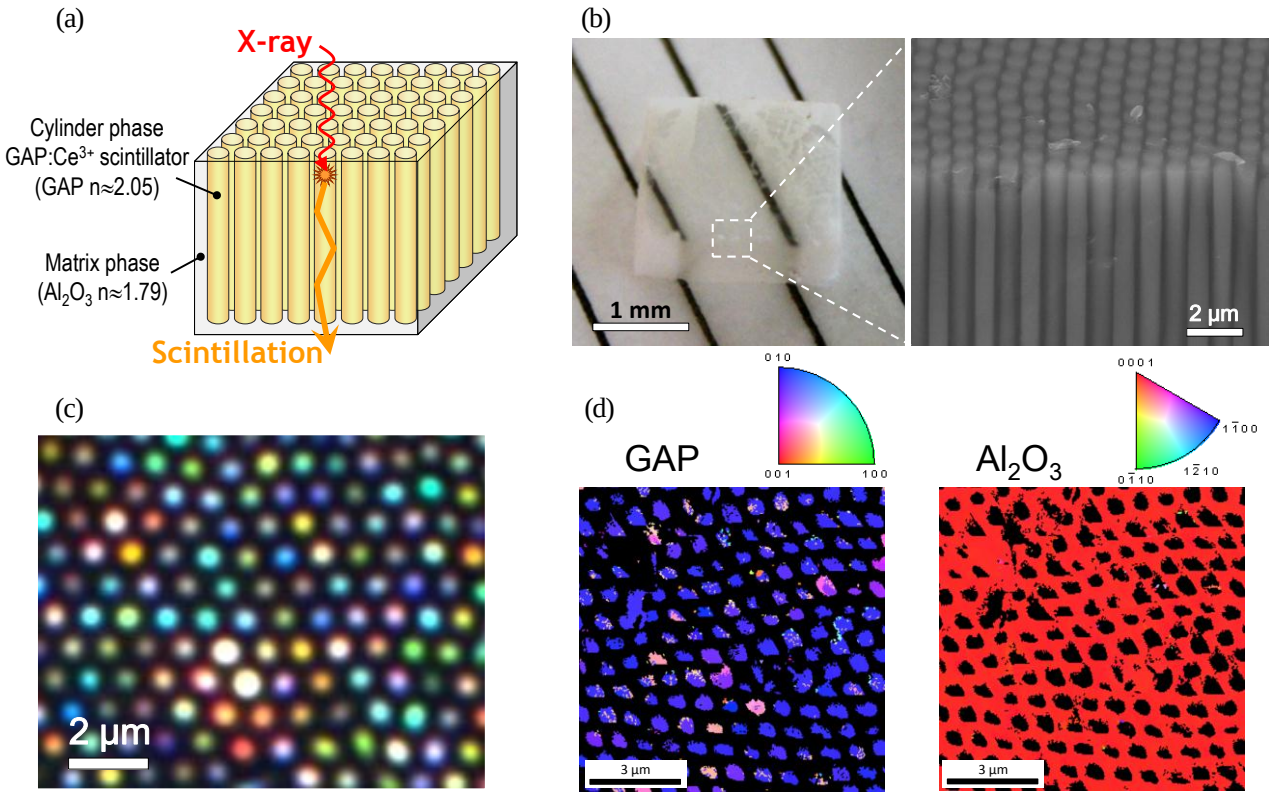

Fig.2. Cylinder-guided GAP-Al_2O_3 PSS: (a) Schematic illustration, (b) appearance and microstructure of the eutectic crystal (c) optical transmission microscope image, and (d) EBSD orientation maps.

Chapter 5. Demonstration of high-resolution X-ray imaging with a GAP- Al_2O_3 PSS

This chapter described the high-resolution X-ray imaging results demonstrated by using the Ce^{3+}-doped GAP-Al_2O_3 PSS. The relationship between the CTF values at 10 lp/mm and the thickness is shown in Fig.3(a). The CTF values of the conventional GOS powder screen (88, 180 μm thick) and the CsI:Tl columnar film (150, 180, 300, 550 μm thick) were also shown for comparison. For the GOS powder screen, the CTF values decreased sharply as the thickness increased, because of strong light scattering. Even though the CsI columnar film had better light guiding properties, the CTF values decreased as the thickness increased, because of the light scattering caused by the surface roughness or imperfections in the crystal. No contrast was observed for samples thicker than 500 μm. Thus, the conventional scintillator suffered from a resolution reduction as its thickness increased because of light scattering. In contrast, the GAP-Al_2O_3 PSS achieved an extremely high resolution, even for scintillators thicker than 1 mm, because of the excellent light guiding properties by the total reflection mode.

Finally, a micrometer-scale resolution X-ray imaging was demonstrated by imaging the gold grating phantoms with a micrometer scale aperture for 150-μm-thick sample as shown in Fig.3(b). The gold grating phantoms had aperture-pitch sizes of 9-22 μm and 4-8.2 μm, respectively. The 9 μm aperture was clearly resolved, and ultimately the 4 μm aperture, corresponding to a bundle of 12 GAP cylinders, was resolved but with low-contrast. The low contrast for the 4 μm aperture can be explained by the propagation of primary photoelectrons and reabsorption of secondary radiation away from the initial position of incident X-ray, and some defects of GAP-Al_2O_3 PSS. This result indicates that GAP-Al_2O_3 PSS may reach the physical resolution limit determined by the material itself.

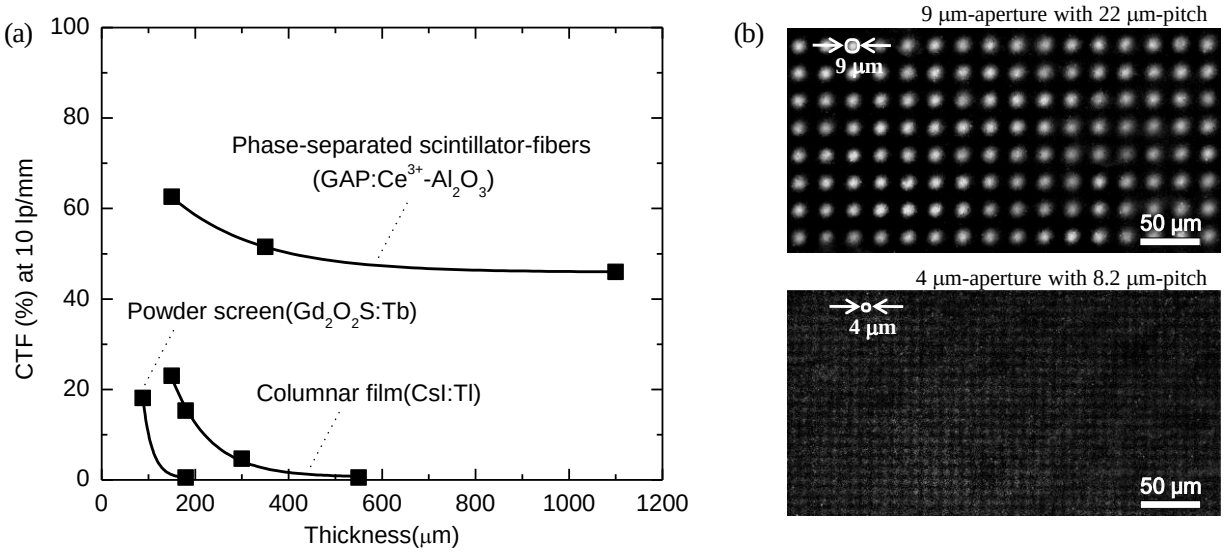

Fig.3. High-resolution X-ray imaging results. (a) CTF values at 10 lp/mm for GAP:Ce^{3+}-Al_2O_3 PSS with various thicknesses. (b) X-ray images of gold grating phantoms with aperture-pitch sizes of 9-22 μm and 4-8.2 μm obtained using a 150 μm thick GAP:Ce^{3+}-Al_2O_3 PSS.

Chapter 6. Conclusion

From this study, various matrix-guided and cylinder-guided PSS were developed from eutectic pairs consist of scintillator materials. Especially, the cylinder-guided GAP-Al_2O_3 PSS enable high-resolution X-ray imaging with micrometer scale regardless of its thickness due to its strictly confined light-guiding behavior in the cylinder phases like an optical fiber. The X-ray imaging system composed of the GAP-Al_2O_3 PSS and miniaturized photo-sensor arrays with micrometer scale pitch can be potentially used for future X-ray imaging applications which require a higher spatial resolution over a wide X-ray energy range.